European Journal of Nuclear Medicine and Molecular Imaging (2019) 46:2152–2162
https://doi.org/10.1007/s00259-019-04392-7

ORIGINAL ARTICLE

^{68}Ga-NOTA-Aca-BBN(7-14) PET imaging of GRPR in children with optic pathway glioma

Jingjing Zhang[1,2,3] · Yongji Tian[4] · Deling Li[5] · Gang Niu[6] · Lixin Lang[6] · Fang Li[1,2] · Yuhan Liu[4] · Zhaohui Zhu[1,2] · Xiaoyuan Chen[6]

Received: 2 February 2019 / Accepted: 4 June 2019 / Published online: 3 July 2019

Abstract

Purpose Optic pathway glioma (OPG) is a rare neoplasm that arises predominantly during childhood. Its location in a sensitive region involving the optic pathways, onset in young patients and controversial therapy choice make the management of OPG a challenge in paediatric neuro-oncology. In this study we assessed gastrin-releasing peptide receptor (GRPR)-targeted positron emission tomography (PET) imaging in children with OPG, and the application of a PET/MRI imaging-guided surgery navigation platform.

Methods Eight children (five boys, mean age 8.81 years, range 5–14 years) with suspicion of optic pathway glioma on MRI were recruited. Written informed consent was obtained from all patients and legal guardians. Brain PET/CT or PET/MRI acquisitions were performed 30 min after intravenous injection of 1.85 MBq/kg body weight of ^{68}Ga-NOTA-Aca-BBN(7-14). Four patients also underwent ^{18}F-FDG brain PET/CT for comparison. All patients underwent surgical resection within 1 week.

Results All 11 lesions (100%) in the eight patients showed prominent ^{68}Ga-NOTA-Aca-BBN(7-14) uptake with excellent contrast in relation to surrounding normal brain tissue. Tumour-to-background ratios (SUVmax and SUVmean) were significantly higher for ^{68}Ga-NOTA-Aca-BBN(7-14) than for ^{18}F-FDG (28.4 ± 5.59 vs. 0.47 ± 0.11 and 18.3 ± 4.99 vs. 0.35 ± 0.07, respectively). Fusion images for tumour delineation were obtained in all patients using the PET/MRI navigation platform. All lesions were pathologically confirmed as OPGs with positive GRPR expression, and 75% were pilocytic astrocytoma WHO grade I and 25% were diffuse astrocytoma WHO grade II. There was a positive correlation between the SUV of ^{68}Ga-NOTA-Aca-BBN(7-14) and the expression level of GRPR ($r^2 = 0.56$, $P < 0.01$, for SUVmax; $r^2 = 0.47$, $P < 0.05$, for SUVmean).

Conclusion This prospective study showed the feasibility of ^{68}Ga-NOTA-Aca-BBN(7-14) PET in children with OPG for tumour detection and localization. ^{68}Ga-NOTA-Aca-BBN(7-14) PET/MRI may be helpful for assisting surgery planning in OPG patients with severe symptoms, GRPR-targeted PET has the potential to provide imaging guidance for further GRPR-targeted therapy in patients with OPG.

Keywords Optic pathway glioma (OPG) · ^{68}Ga-NOTA-Aca-BBN(7-14) · Paediatric neuro-oncology · PET · PET/MRI · Gastrin-releasing peptide receptor (GRPR)

Jingjing Zhang, Yongji Tian and Deling Li contributed equally to this work.

This article is part of the Topical Collection on Infection and inflammation.

✉ Zhaohui Zhu
zhuzhh@pumch.cn

✉ Xiaoyuan Chen
shawn.chen@nih.gov

[1] Department of Nuclear Medicine, Peking Union Medical College Hospital, Chinese Academy of Medical Sciences and Peking Union Medical College, Beijing 100730, China

[2] Beijing Key Laboratory of Molecular Targeted Diagnosis and Therapy in Nuclear Medicine, Peking Union Medical College (PUMC) Hospital, Chinese Academy of Medical Science and PUMC, Beijing 100730, China

[3] THERANOSTICS Center for Molecular Radiotherapy and Precision Oncology, Zentralklinik Bad Berka, 99437 Bad Berka, Germany

[4] Department of Pediatric Neurosurgery, Beijing Tiantan Hospital, Capital Medical University, Beijing Key Laboratory of Brain Tumor, Beijing 100730, China

[5] Department of Neurosurgery, Beijing Tiantan Hospital, Capital Medical University, Beijing Key Laboratory of Brain Tumor, Beijing 100730, China

[6] Laboratory of Molecular Imaging and Nanomedicine (LOMIN), National Institute of Biomedical Imaging and Bioengineering (NIBIB), National Institutes of Health (NIH), Bethesda, MD 20892, USA

Introduction

Optic pathway glioma (OPG) is a rare neoplasm that arises predominantly during childhood [1, 2]. It comprises approximately 2% of all central nervous system tumours and accounts for approximately 3–5% of paediatric brain tumours [3, 4]. In approximately 15–20% of patients, OPG occurs concurrently with neurofibromatosis type 1 (NF-1) [5, 6]. OPG can occur in the intraorbital optic nerve, intracanalicular optic nerve, intracranial optic nerve, optic chiasma, optic tract, lateral to the geniculate body and hypothalamus, and adjacent to the visual pathway and hypothalamus. Its location in sensitive regions involving the optic pathways, onset in young patients, and controversial therapy choice make the management of OPG a challenge in paediatric neuro-oncology [7].

Early diagnosis and appropriate management led by a multidisciplinary team remains the standard of care for OPG patients [8, 9]. Although pathologically, OPGs are often identified as low-grade gliomas [2, 10] with pilocytic astrocytoma and pilomyxoid astrocytoma being the main pathological types, the clinical course of OPG is unpredictable and growth patterns are irregular. Some patients also experience progression with rapid visual loss and worsening symptoms associated with increased tumour size. Long-term survival can be achieved in selected patients with OPGs using tailored treatment.

However, approaches to providing adequate therapy are controversial, and include surveillance, chemotherapy, surgery and radiotherapy. Chemotherapy has been recommended as the first-line treatment for OPG in recent years [11, 12]. Although data are still limited, several studies have also indicated that surgery should be used to control tumour progression [13, 14], especially in children with large OPG volumes and symptoms of functional impairment and obstructive hydrocephalus [15]. Management of these lesions needs to be highly individualized. OPG patients often show a variety of clinical symptoms, such as vision loss, endocrine disorders and intracranial hypertension, making decisions about treatment options more difficult. Further, there is a lack of optimal imaging surveillance or proper visualization of tumour biology of OPGs at the molecular level.

Gastrin-releasing peptide receptor (GRPR), also known as bombesin receptor subtype 2, is a member of the G protein-coupled receptor family, which has been found to be overexpressed in various types of cancer, including prostate cancer, breast cancer, glioma, colorectal cancer, lung cancer, renal cell cancer and gastrointestinal stromal tumours [16–18]. Therefore, GRPR has become a promising target for receptor-mediated tumour imaging and therapy with radiolabelled peptide analogues [19–25]. The presence of GRPR has been pathologically confirmed in specimens of all grades of human glioma [26]. We have previously used the GRPR-targeting molecular probe ^{68}Ga-NOTA-Aca-BBN(7-14) in positron-emission tomography (PET) imaging of both low-grade and high-grade glioma [27]. By conjugating ^{68}Ga-NOTA-Aca-BBN(7-14) with a near-infrared fluorophore IRDye800CW, we have also developed a dual-modality PET/optical imaging probe ^{68}Ga-IRDye800CW-BBN [28] to specifically image GRPR expression in glioblastoma multiforme (GBM) both preoperatively and using real-time optical navigation intraoperatively to achieve maximal safe resection of GBM.

In this study we assessed GRPR-targeted PET imaging in children with OPG, using ^{18}F-FDG PET for comparison. We also assessed the application of a multimodality ^{68}Ga-NOTA-Aca-BBN(7-14)-PET/MRI imaging-guided surgery navigation platform.

Materials and methods

Patient recruitment

This study was approved by the Ethics Committee of Peking Union Medical College Hospital, Peking Union Medical College, Chinese Academy of Medical Sciences, and registered online at the US National Institutes of Health ClinicalTrials.gov (ID NCT02520882). Written informed consent was obtained from all patients and legal guardians. All procedures were in accordance with the ethical standards of the institutional and national research committees and with the principles of the 1964 Declaration of Helsinki and its later amendments or comparable ethical standards.

Eight children (five boys, three girls; age range 5–14 years, mean age 8.81 ± 4.64 years) with suspicion of OPG on contrast-enhanced MRI took part in the study. The inclusion criteria included: less than 18 years old, having optic pathway neoplasm(s) identified on MRI, severe symptoms, large tumour, or disease progression and therefore surgery recommended as the initial intervention [15]. The exclusion criteria included: less than 3 years old, claustrophobia, kidney or liver failure, and inability to complete the study. All tumours were classified according to the Dodge classification [29]: *stage 1* involvement of only the optic nerve, *stage 2* involvement of the optic chiasm, with or without optic nerve involvement, and *stage 3* involvement of the hypothalamus and/or adjacent structures. All patients underwent surgical resection within 1 week with PET/MRI image fusion and the use of the navigation platform. Postoperative MRI was performed within 2 weeks of surgery to determine the extent of surgical resection. The demographics of the patients at baseline are given in Table 1.

Radiopharmaceuticals

^{68}Ga-NOTA-Aca-BBN(7-14) was synthesized following a procedure reported previously [27]. In brief, the precursor

NOTA-Aca-BBN(7-14) was dissolved in deionized water to 1 mg/mL and stored at 4 °C before use. ^{68}Ga was eluted from a ^{68}Ge/^{68}Ga generator (Eckert & Ziegler, Berlin, Germany) using 0.05 M HCl and mixed with 1.25 M NaOAc buffer to adjust the pH to 4.0. The mixture was then directly transferred to a 1-mL plastic tube containing 30 mg of NOTA-Aca-BBN(7-14). After shaking, the mixture was incubated on a heating block at 100 °C for 10 min. The quality control was performed by thin layer chromatography (Bioscan, Washington DC, USA) with CH_3OH/NH_4OAc (1:1 v/v) as the developing solution. The radiochemical purity of the product was over 97%. The product was dissolved in 0.9% saline and passed through a 0.22 μm filter to ensure sterility.

Examination procedures

Brain PET/CT (five patients) or PET/MRI (three patients) acquisitions were performed 30 min after bolus injection of ^{68}Ga-NOTA-Aca-BBN(7-14). The dosage was based on the body weight of the child (33.3–90.7 MBq, 1.85 MBq/kg body weight).

^{68}Ga-GRPR PET/CT

All patients underwent ^{68}Ga-NOTA-Aca-BBN(7-14) PET/CT scans using a Siemens Biograph 64 TruePoint system. No fasting, special diet, hydration or other specific preparation was required on the day of ^{68}Ga-BBN PET/CT. A low-dose CT scan (120 kV, 35 mA, 3-mm layer, 512 × 512 matrix, 70-cm field of view) was obtained, followed 30 min after ^{68}Ga-NOTA-Aca-BBN(7-14) injection by a 10-min PET acquisition covering the whole head of the patient. The images were transferred to a MMWP workstation (Siemens) for analysis. One patient also underwent whole-body PET/CT (from the top of the skull to the middle of the femur). After a low-dose CT scan, whole-body PET was performed with 2 min per bed position (four bed positions according to the height of the patient).

^{68}Ga-GRPR PET/MRI

The images were acquired using a Signa time-of-flight PET/MRI system (GE Healthcare). Simultaneous PET and 3-T MRI data were acquired [30]. A 0.1 mmol/kg bolus of gadopentetate dimeglumine contrast agent was administered using a power injector at a rate of 3 mL/s. Coronal and sagittal fat-saturation CUBE T1-weighted imaging was then performed. All sequences in this examination covered the whole head, including the optic tract and sellar region. For the integrated PET/MRI scan, attenuation correction was performed with T1-weighted imaging, and PET acquisition was performed before and after injection of contrast agent. The ^{68}Ga-NOTA-Aca-BBN(7-14) PET/MRI studies were reviewed for regions of increased uptake independently by two board-certified specialists in nuclear medicine, who were masked to the clinical data.

Other examinations

Preoperative contrast-enhanced MRI was performed during the week before surgery. All MR scans were performed on a 3.0 T scanner with a head coil, and 0.1 mmol/kg body weight

Table 1 Patient demographics

Patient no.	Gender	Age (years)	Clinical manifestation	Neurofibromatosis type 1 status	Tumour location	Dodge stage
1	Male	5	Decreased vision (right eye), blindness (left eye), eye movement disorders, nausea, vomiting	No	Optic chiasma, optic tract, adjacent to the visual pathway, suprasellar cistern, hypothalamus	3
2	Male	13	Headache, nausea, vomiting, disturbance of consciousness, mild decreased vision, slow light reflection	No	Optic chiasma, hypothalamus, suprasella cistern, third ventricle	3
3	Female	5	Decreased vision, nystagmus, strabismus, diplopia, nausea, vomiting	No	Intracranial optic nerve, optic chiasma, optic tract, lateral geniculate body, adjacent to the visual pathway	2
4	Female	5	Decreased vision, slow light reflection, nausea, vomiting, endocrinology symptoms	No	Optic chiasma, hypothalamus	3
5	Male	7	Decreased vision (right eye), blindness (left eye), nystagmus, strabismus, diplopia, eye movement disorders	No	Intracranial optic nerve, optic chiasma, optic tract	2
6	Male	14	Headache, decreased vision	No	Optic chiasma, optic tract	2
7	Male	6	Fever, nausea, vomiting, consciousness disturbances	No	Hypothalamus, third ventricle	3
8	Female	5	Progressively decreasing vision (right eye)	No	Hypothalamus, right side of parasellar regions	3

Magnevist was injected intravenously. Slice thickness was 5 mm. The postoperative MRI, which was performed within 2 weeks of surgery, was used to determine the extent of surgical resection using the following specific assessment definitions: near-total resection (removal of more than 90% of the tumour), subtotal resection (removal of 50–90% of the tumour), and partial resection (removal of less than 50% of the tumour). Four patients also underwent ^{18}F-FDG brain PET/CT within 3 days for comparison.

Image and data analysis

A Siemens MMWP workstation was used for postprocessing. In the five patients who underwent ^{68}Ga-NOTA-Aca-BBN(7-14) PET/CT, the PET images were coregistered to the MR images with automatic image registration and manual positioning. In all patients, visual analysis was used to determine the general biodistribution and the temporal and intersubject stability. The reference normal brain region was defined as contralateral white/grey matter, in the constant proportion of white and grey based on MR imaging and out of the midline, ventricle and great vessels. Volumes of interest for normal brain tissues were drawn using three-dimensional ellipsoid isocontouring, and the radioactivity concentrations and standardized uptake values (SUVs) in these volumes of interest were obtained using the workstation software. Regions of interest were drawn manually on the brain lesions concerned with the assistance of the corresponding CT and MRI images. The molecular tumour volume (MTV) obtained on ^{68}Ga-NOTA-Aca-BBN(7-14) PET was defined and calculated as the total number of voxels with a threshold of ≥40% of the SUVmax in the volume of interest. The results are expressed as SUVmean and SUVmax. MR and PET images were compared and then fused to visualize the uptake area and to adjust the boundaries.

Pathological analysis

All patients underwent surgical removal of their tumour within 1 week of ^{68}Ga-NOTA-Aca-BBN(7-14) PET. The pathology was determined by three neuropathologists separately, and in the case of discrepancy, consensus was reached by another higher-level pathologist. The criteria used for the pathological diagnosis were the 2016 World Health Organization Classification of Tumors of the Central Nervous System (CNS WHO) [31]. Further, tumour samples were fixed with 10% neutral buffered formalin and embedded in paraffin. After blocking and washing, 5-mm-thick tissue sections were incubated with rabbit antihuman polyclonal antibody against human GRPR (PA5-256791; Thermo Fisher Scientific). After washing with phosphate-buffered saline, each section was incubated with horseradish peroxidase-conjugated antirabbit IgG for 60 min at room temperature. Diaminobenzidine was used as the chromogen, and the slides were counterstained with haematoxylin and eosin. The stained slides were examined using a light microscope (BX41; Olympus). For semiquantification of GRPR expression, five entire high-power fields (×40) per slide containing clusters of malignant cells were identified randomly and scored for intensity and percentage of GRPR staining. The procedure was repeated by two independent, experienced examiners.

Statistical analysis

Statistical analysis was performed using Prism 5.0 software (GraphPad, San Diego, CA). Continuous variables are summarized as means ± standard deviation. Correlations between quantitative parameters were evaluated using Spearman's rank correlation coefficient. *P* values of all statistical tests were two-tailed, and *P* values less than or equal to 0.05 were considered significant.

Results

Biodistribution and tumour uptake of ^{68}Ga-NOTA-Aca-BBN(7-14) in OPG patients

^{68}Ga-NOTA-Aca-BBN(7-14) cleared through the kidneys. The one patient who underwent whole-body PET showed uptake of ^{68}Ga-NOTA-Aca-BBN(7-14) mainly in the pancreas, liver, kidneys, bladder and tumour(s). Uptake was quite low in normal brain tissue, lungs, mediastinum, thorax and skeleton. All 11 lesions in the eight patients showed prominent ^{68}Ga-NOTA-Aca-BBN(7-14) uptake with excellent contrast in relation to surrounding normal brain tissue (Figs. 1 and 2). The SUVmax and SUVmean of all 11 lesions were 1.82 ± 0.59 and 1.17 ± 0.47, respectively. Tumour-to-background (T/B) ratios, defined as the tumour SUVmax to background SUVmean, and tumour SUVmean to background SUVmean, were 28.4 ± 5.59 and 18.3 ± 4.99, respectively.

Comparison between ^{68}Ga-NOTA-Aca-BBN(7-14) PET/CT and ^{18}F-FDG PET/CT

Low ^{18}F-FDG uptake in tumour lesions was observed on ^{18}F-FDG PET/CT. The calculated SUVmean and SUVmax of ^{18}F-FDG were 3.60 ± 1.09 (range 1.98–4.3) and 4.83 ± 1.51 (range 2.65–5.90), respectively. T/B ratios were 0.47 ± 0.11 and 0.35 ± 0.07 based on SUVmax and SUVmean, respectively. The T/B uptake for ^{18}F-FDG was opposite to that for ^{68}Ga-NOTA-Aca-BBN(7-14) and the T/B ratio for ^{18}F-FDG PET was much lower than that for ^{68}Ga-NOTA-Aca-BBN(7-14) (0.47 ± 0.11 vs. 28.4 ± 5.59, $P < 0.001$; Fig. 1).

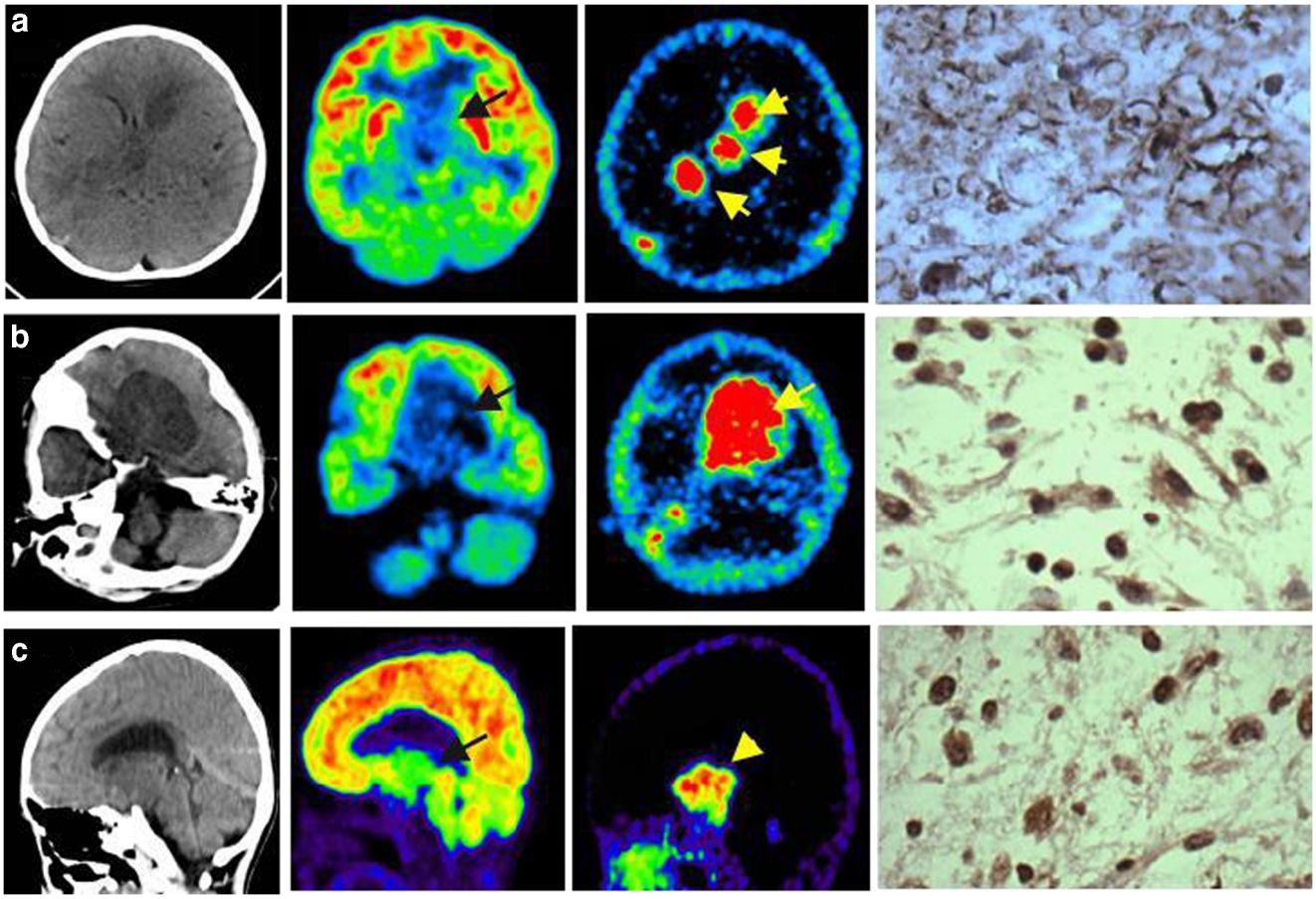

Fig. 1 Representative brain CT images (*left*), ^{18}F-FDG PET images (*second column*), ^{68}Ga-NOTA-Aca-BBN(7-14) PET images (*third column*) and immunohistochemically stained tissue sections (*right*, ×400) in patients with optic pathway glioma (*arrows*). **a** A 5-year-old girl (Table 1, patient 3) with multiple space-occupying lesions with a diagnosis of diffuse astrocytoma (WHO grade II). The Dodge classification was stage 2. The SUVmax of the lesions was 2.05 and the SUVmean was 1.45. Tumour-to-background (T/B) ratios were 30.9 and 20.2 based on SUVmax and SUVmean, respectively, and the lesions showed positive staining for GRPR. **b** A 5-year-old girl (Table 1, patient 4) with OPG with a pathological diagnosis of pilocytic astrocytoma (WHO grade I). The Dodge classification was stage 3. The SUVmax was 2.71 and the SUVmean was 2.00. T/B ratios were 22.9 and 17.5 based on SUVmax and SUVmean, respectively, and the lesion showed positive staining for GRPR. **c** A 13-year-old boy (Table 1, patient 2) with OPG with a pathological diagnosis of pilocytic astrocytoma (WHO grade I). The Dodge classification was stage 3. The SUVmax and SUVmean were 1.70 and 1.01. The T/B ratios were 29.9 and 19.3 based on SUVmax and SUVmean, respectively, and the lesion showed positive staining for GRPR

Multimodality ^{68}Ga-NOTA-Aca-BBN(7-14) PET/MRI navigation guided surgery for OPG

PET/MRI fusion images were obtained in all eight patients and successfully used in the PET/MRI navigation platform for tumour delineation (Figs. 3 and 4). Three patients underwent simultaneous PET/MRI. All 11 lesions showed isointensity to hypointensity on T1-weighted images and hyperintensity on T2-weighted images, and heterogeneous (nine lesions) or homogeneous (two lesions) enhancement after administration of Gd contrast agent. In four patients the MTV on ^{68}Ga-NOTA-Aca-BBN(7-14) PET (using a threshold of ≥40% of the SUVmax in the volume of interest) matched the tumour volume on MRI (T2-weighted and fluid-attenuated inversion recovery, FLAIR, tumour volume), in three patients the area of accumulation of ^{68}Ga-NOTA-Aca-BBN(7-14) on PET was smaller than the area on MRI (Table 2, Fig. 4), and in one patient the area of accumulation of ^{68}Ga-NOTA-Aca-BBN(7-14) on PET was larger than the area on MRI (Table 2). The most common tumour location in this series was the hypothalamus (Dodge stage 3, 62.5%), followed by the optic chiasm (Dodge stage 2, 37.5%), and no patient had Dodge stage 1 tumour. In six patients (75%) subtotal resection (50–90%) was achieved, and in two patients (25%) near-total resection (>90%) was achieved, with multimodality imaging and neuronavigation assistance.

Correlation with GRPR expression

The final pathological evaluation confirmed that all lesions were OPGs. Of the eight patients, six (75%) were diagnosed with pilocytic astrocytoma World Health Organization

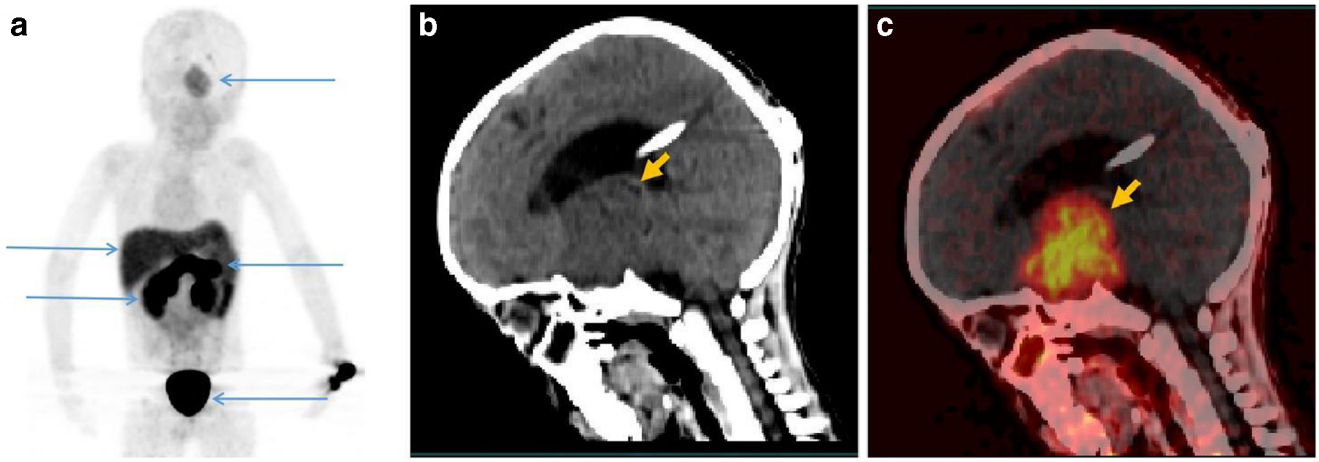

Fig. 2 PET/CT imaging in a 5-year-old boy (Table 1, patient 1). **a** Whole-body maximum intensity projection PET image 30 min after intravenous administration of ^{68}Ga-NOTA-Aca-BBN(7-14). Uptake is seen mainly in the tumour, liver, pancreas, kidneys and bladder (*blue arrows*, from top to bottom, respectively). **b**, **c** Sagittal CT image (**b**) and fusion PET/CT image (**c**) show strong ^{68}Ga-NOTA-Aca-BBN(7-14) uptake in the tumour lesion (*orange arrows*) that involves the optic chiasma, optic tract, adjacent the visual pathway, suprasella cistern and hypothalamus. The SUVmax of the tumour lesion was 2.75 and the SUVmean was 1.73. The tumour-to-background (T/B) ratios were 31.0 and 20.3 based on SUVmax and SUVmean, respectively. Postoperative pathology after subtotal resection was pilocytic astrocytoma, WHO grade I, with positive staining for GRPR

(WHO) grade I, and the other two (25%) with diffuse astrocytoma, WHO grade II. Immunohistochemical staining was positive for GRPR expression in all 11 samples from the eight patients (Fig. 3). There was a positive correlation between the SUV of ^{68}Ga-NOTA-Aca-BBN(7-14) and the expression level of GRPR ($r^2 = 0.56$, $P < 0.01$, for SUVmax; $r^2 = 0.47$, $P < 0.05$, for SUVmean; Fig. 3).

Postoperative treatment and follow-up

There was no surgery-associated mortality and there were no severe complications in any of the patients. Convulsions and seizures in one patient occurred during hospitalization. Transient electrolyte disturbances were observed in three patients. Seven patients (87.5%) received three-dimensional conformal radiotherapy (3DCRT) after surgery (Table 2). Two patients received chemotherapy after surgery. No serious complications associated with surgery combined with radiotherapy were observed in any of the patients. No patient died or had tumour recurrence during the follow-up period (10–15 months). In all the patients the tumour mass was controlled and the clinical outcome was improved (Fig. 5), Five of seven patients had stable or improved vision, and five of five had remission of hydrocephalus.

Discussion

GRPR is an attractive target for tumour diagnosis and radionuclide therapy with radiolabelled peptide analogues in cancers such as prostate cancer, breast cancer and glioma. In a study evaluating the presence of GRPR in glioma, 100% of glioma specimens analysed by immunohistochemistry were GRPR-positive [26]. In this study, positive GRPR expression and high corresponding accumulation of ^{68}Ga-NOTA-Aca-BBN(7-14) were present in all the OPGs, which were

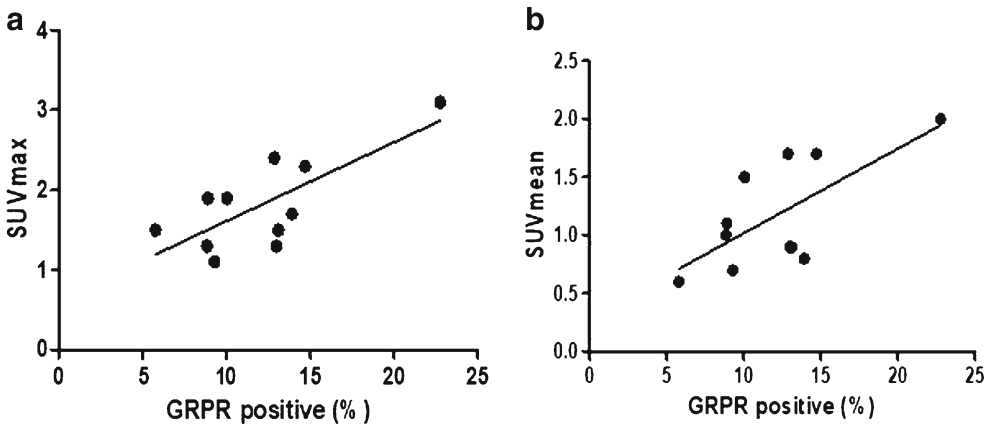

Fig. 3 Correlations between SUV (**a** SUVmax, **b** SUVmean) of ^{68}Ga-NOTA-Aca-BBN(7-14) and GRPR expression level determined by immunohistochemical staining ($r^2 = 0.56$, $P < 0.01$, for SUVmax; $r^2 = 0.47$, $P < 0.05$, for SUVmean)

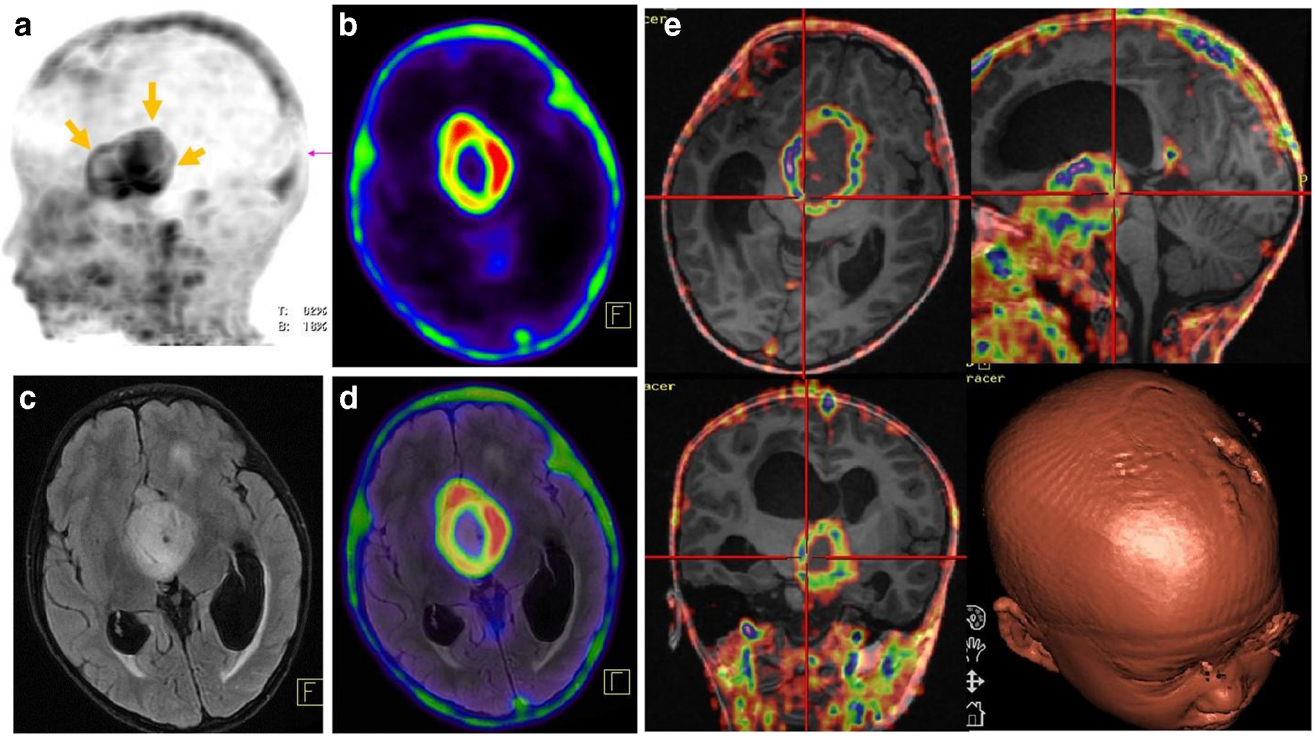

Fig. 4 PET/MRI imaging in a 6-year-old boy (Table 1, patient 7): **a** sagittal maximum intensity projection PET brain image at 30 min after intravenous administration of ^{68}Ga-NOTA-Aca-BBN(7-14); **b** representative ^{68}Ga-NOTA-Aca-BBN(7-14) PET image (MTV 39,667 mm^3); **c** MR image (tumour volume 63,648 mm^3); **d** PET/MRI fusion image (subtotal resection was performed partially assisted by multimodality imaging and neuronavigation); **e** representative ^{68}Ga-NOTA-Aca-BBN(7-14) PET/MRI fusion image on the navigation platform

pathologically low-grade gliomas (pilocytic astrocytoma WHO grade I, and diffuse astrocytoma WHO grade II). Remarkably high tumour uptake of ^{68}Ga-NOTA-Aca-BBN(7-14) as compared with extremely low uptake in the surrounding normal brain tissues provides the molecular basis for diagnostic imaging in OPGs and indicates the value of ^{68}Ga-NOTA-Aca-BBN(7-14) PET for this application.

Approximately 90% of OPGs occur in children. OPGs in children are most commonly benign with slow growth, whereas OPGs in adults are usually malignant with a high grade and include glioblastoma (WHO grade IV) [9]. There are limited data concerning brain ^{18}F-FDG PET imaging in OPG. Miyamoto et al. reported one case of adult malignant OPG in the optic tract that showed high uptake of ^{18}F-FDG [32]. The histological diagnosis was astrocytoma WHO grade III. In our series, visually much lower uptakes of ^{18}F-FDG were observed in children with pathologically confirmed WHO grade I and WHO grade II OPG. The semiquantitative analysis showed that SUVmax was slightly higher than in a previous study [33] in children with NF-1 (in 62.5% of the patients SUVmax was <3), which was probably because all the patients in our study had progressive disease before surgery.

MRI is considered the mainstay of radiological diagnostic imaging in children with OPG [2, 34] with thin slices and high resolution of the optic nerves and optic chiasm. However, currently, no MRI criteria can predict tumour growth and prognosis, and MRI measurements for OPGs have not been standardized [35]. A typical MRI appearance is considered an isointense to mildly hypointense lesion on T1-weighted images, hyperintensity on T2-weighted images, and homogeneous enhancement [2, 36]. All 11 lesions in our study matched well with the conventional appearance of T1-weighted and T2-weighted images. However, enhancement was variable and the majority of lesions were heterogeneous, and showed cystic components, which are more common in OPG patients with sporadic disease than in NF-1 patients [11, 37, 38]. In 7 of the 11 lesions (63.6%) in four of eight patients (50%) the MTV on ^{68}Ga-NOTA-Aca-BBN(7-14) GRPR PET matched the tumour volumetric measurement on MRI (T2-weighted images). Maloney et al. reported that T2/FLAIR sequences and gadolinium-enhanced sequences were similar, with increased tumour size as the only common feature that was apparent on both gadolinium contrast-enhanced images and non-contrast T2 sequence images [39]. However, in our study, we also observed that tumour volume on non-contrast T2 and enhanced MRI did not exactly match in 3 of the 11 lesions (27.3%). These findings indicate the heterogeneity of OPGs and the significance of multimodality imaging in OPGs.

In our previous study, we evaluated a large series of surgical treatments in children with OPG and found that intratumoral

Table 2 Multimodality imaging, treatment characteristics and follow-up of the children with symptomatic OPG

Patient no.	MRI findings	Tumour volume on MRI (mm^3)	MTV on GRPR PET (mm^3)	Pathology	WHO grade	Resection extent	Postoperative radiotherapy	Postoperative chemotherapy	Follow-up period (months)	Follow-up results
1	Hyperintensity on T2, heterogeneous enhancement	153,700	153,700	Pilocytic astrocytoma	I	Subtotal resection (70–90%)	Yes	No	11	Tumour remission, stable vision, hydrocephalus remission, hyponatraemia
2	Hyperintensity on T2, heterogeneous enhancement	105,248	103,224	Pilocytic astrocytoma	I	Near-total resection (>90%)	Yes	No	15	Tumour remission, hydrocephalus remission, vision improved, hyponatraemia
3	Hyperintensity on T2, heterogeneous enhancement	132,670	132,670	Diffuse astrocytoma	II	Subtotal resection (50–70%)	No	Yes	14	Tumour remission, vision improved, developmental delay
4	Hyperintensity on T2, heterogeneous enhancement	72,960	72,960	Pilocytic astrocytoma	I	Subtotal resection (50–70%)	Yes	No	15	Tumour remission, hydrocephalus remission, hyponatraemia, memory deterioration, developmental delay
5	Hyperintensity on T2, homogeneous enhancement	28,710	31,465	Pilocytic astrocytoma	I	Subtotal resection (50–70%)	Yes	No	15	Tumour remission, stable vision
6	Hyperintensity on T2, homogeneous enhancement	55,965	55,965	Pilocytic astrocytoma	I	Subtotal resection (50–70%)	Yes	No	12	Tumour remission, decreased vision
7	Hyperintensity on T2, heterogeneous enhancement	63,648	39,667	Diffuse astrocytoma	II	Subtotal resection (50–70%)	Yes	No	12	Tumour remission, hydrocephalus remission, hyponatraemia
8	Hyperintensity on T2, heterogeneous enhancement	25,179	24,101	Pilocytic astrocytoma	I	Near-total resection (>90%)	Yes	Yes	10	Tumour remission, vision improved, hyponatraemia

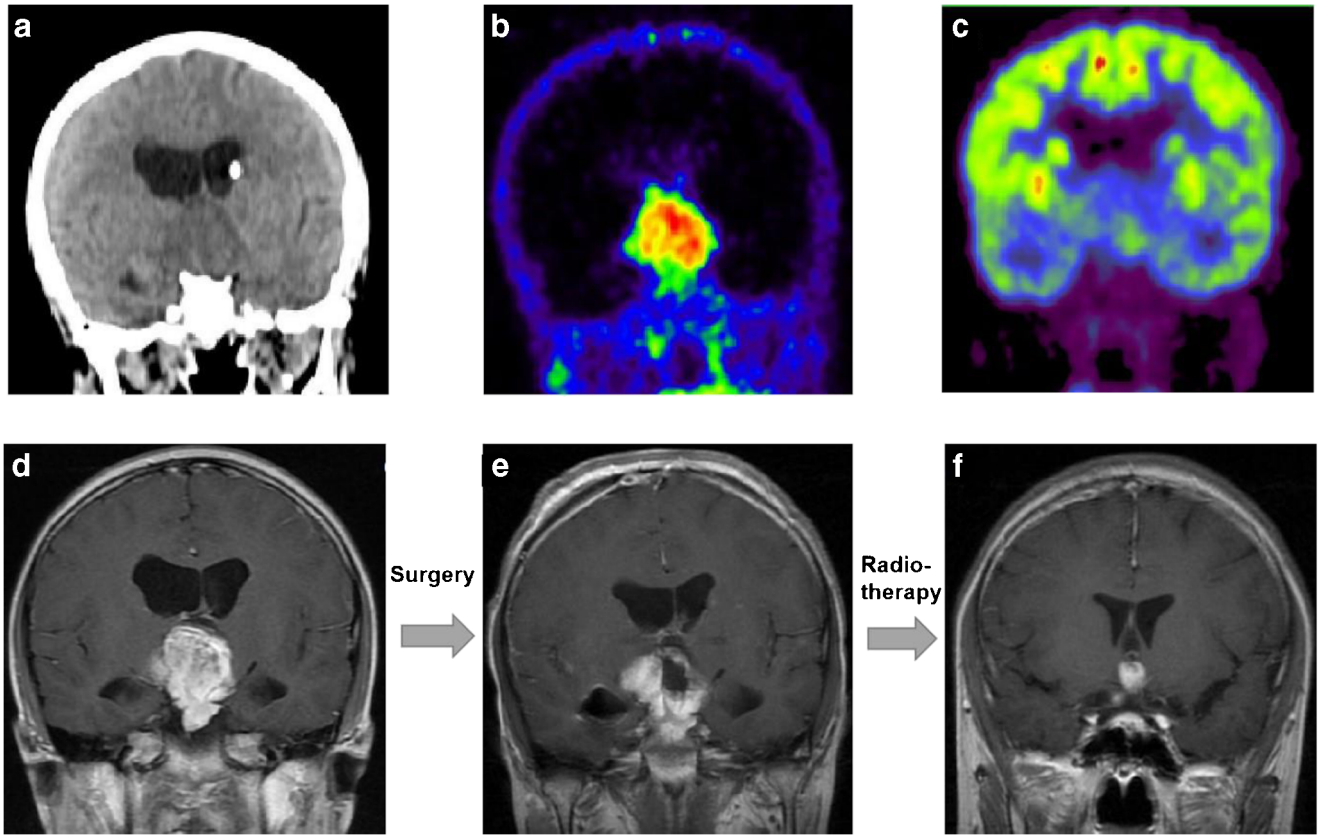

Fig. 5 Preoperative and postoperative coronal brain imaging in a 13-year-old boy with OPG. **a–d** Preoperative images: **a** CT, **b** ^{68}Ga-NOTA-Aca-BBN(7-14) PET, **c** ^{18}F-FDG PET, **d** T1-weighted enhanced MRI. The tumour involves the optic chiasma, hypothalamus, suprasella cistern and third ventricle, with Dodge stage 3. The initial symptoms were headache, nausea, vomiting, disturbance of consciousness and slow light reflection. He underwent near-total resection (>90%) assisted by multimodality imaging and neuronavigation. Postoperative pathology after subtotal resection was pilocytic astrocytoma, WHO grade I. **e**, **f** Postoperative MRI images. **e** The image obtained 13 days after surgery shows satisfactory lesion resection. The patient subsequently received radiotherapy. **f** The image obtained 12 months after surgery shows remission of the tumour and hydrocephalus. Vision and normal activities of daily living had also improved

partial resection was preferable to total resection [15]. We advocate the use first of partial intra-tumoral resection in symptomatic OPG patients under the guidance of a neuronavigation system which has been gradually introduced to improve the safety and accuracy of surgery. The main goal of surgery in OPG patients is cytoreduction by reducing the tumour mass, and the achievement of a definite histological diagnosis for the guidance of the subsequent radiotherapy or chemotherapy, and meanwhile decreasing obstructive hydrocephalus. In this study, all patients had large-volume OPGs, presented with worsening symptoms and required surgical intervention. The most common clinical manifestation was visual deficit (87.5%), including decreased vision or blindness, eye movement disorders, intracranial hypertension (75.0%), endocrinology symptoms (37.5%), and other neurological symptoms (12.5%). No patient deaths associated with surgery or severe complications were observed. The application of intraoperative navigation techniques improved surgical skill and safety. ^{68}Ga-NOTA-Aca-BBN(7-14) PET/MRI clearly defined the location and delineation of the tumour. PET/MRI was more beneficial in OPG patients than PET/CT not only in identifying the extent of invasion of the tumour and determining which surrounding structures were likely to be involved but also in providing anatomical data which is the strength of MRI. Using a hybrid simultaneous PET/MRI system helped access the inherent advantages of the precise fusion of PET image and high-grade anatomical MR images or even the functional parameters of multiparametric MRI information, and was also more convenient for the paediatric patients than conducting MRI and PET examinations independently.

^{68}Ga-NOTA-Aca-BBN(7-14) PET/MRI was able to offer more advantages over PET/CT in characterizing and precise delineation of the tumour to guide surgery in the children with OPG. For those tumours with heterogeneous uptake of ^{68}Ga-NOTA-Aca-BBN(7-14) or heterogeneous enhancement after Gd contrast agent administration in MRI, intraoperative navigation diffusion tensor tractography was also performed to define the visual pathway, which effectively guided the operation and thus greatly reduced the risk of visual loss related to surgery. Most of the children underwent subtotal resection of the tumour or partial intratumoral resection (around 70%). After surgery, all patients were in good condition before discharge. The surgical treatment controlled tumour progression

in eight of eight patients (100%) with no recurrence in 10–15 months. Postoperatively, seven patients (87.5%) showed improved or stable visual outcomes and had no serious complications, and six patients (75%) were able to go to school during the follow-up period.

Due to options for incomplete surgical resection in OPG patients, appropriate safety margins should be carefully applied to avoid damage to normal optic nerves, and subsequent treatment is needed, such as adjuvant radiotherapy. The confirmed overexpression of GRPR in OPGs and the high uptake of ^{68}Ga-NOTA-Aca-BBN(7-14) on PET imaging also indicates the potential of GRPR-targeted radiotherapy in OPG patients. The expected value might correlate with SUVs derived from ^{68}Ga-NOTA-Aca-BBN(7-14) PET. Further investigations are warranted.

This study suffered from several limitations. The number of patients was too small to show that GRPR is expressed in all OPGs despite 100% positivity in this pilot study. There could also have been a selection bias, as all children included in this study had large tumours and disease progression, and none of the children had NF-1. The assessment of efficacy and safety of surgery with intraoperative navigation was insufficient due to the short follow-up and the fact that all patients also received postoperative radiotherapy or chemotherapy, including three-dimensional conformal radiotherapy after surgery that was recommended in children older than 5 years. Although GRPR PET imaging showed the heterogeneity of OPGs, deep molecular biology analysis of the specimens of OPG was limited. Further analysis and more clinical studies in a larger group of patients are needed.

Conclusion

This prospective study indicated the feasibility of ^{68}Ga-NOTA-Aca-BBN(7-14) PET for tumour detection, localization and differentiation in children with OPG. Multimodality ^{68}Ga-NOTA-Aca-BBN(7-14) PET/MRI may be helpful in assisting surgery planning in OPG patients with severe symptoms. GRPR PET has the potential to provide imaging guidance for further GRPR-targeted therapy in children with OPG.

Acknowledgments This work was supported in part by the Intramural Research Program (IRP) of the National Institute of Biomedical Imaging and Bioengineering (NIBIB), the National Institutes of Health (NIH), and the National Natural Science Foundation of China (81701742).

Compliance with ethical standards

Conflicts of interest None.

Statement of human rights All procedures performed in studies involving human participants were in accordance with the ethical standards of the institutional and/or national research committee and with the principles of the 1964 Declaration of Helsinki and its later amendments or comparable ethical standards.

Informed consent Informed consent was obtained from all individual participants included in the study and their legal guardians.

References

1. Ertiaei A, Hanaei S, Habibi Z, Moradi E, Nejat F. Optic pathway gliomas: clinical manifestation, treatment, and follow-up. Pediatr Neurosurg. 2016;51:223–8. https://doi.org/10.1159/000445064.
2. Park ES, Park JB, Ra YS. Pediatric glioma at the optic pathway and thalamus. J Korean Neurosurg Soc. 2018;61:352–62. https://doi.org/10.3340/jkns.2018.0040.
3. Aihara Y, Chiba K, Eguchi S, Amano K, Kawamata T. Pediatric optic pathway/hypothalamic glioma. Neurol Med Chir (Tokyo). 2018;58:1–9. https://doi.org/10.2176/nmc.ra.2017-0081.
4. D'Arco F, Culleton S, De Cocker LJL, Mankad K, Davila J, Tamrazi B. Current concepts in radiologic assessment of pediatric brain tumors during treatment, part 1. Pediatr Radiol. 2018;48:1833–43. https://doi.org/10.1007/s00247-018-4194-9.
5. Listernick R, Ferner RE, Liu GT, Gutmann DH. Optic pathway gliomas in neurofibromatosis-1: controversies and recommendations. Ann Neurol. 2007;61:189–98. https://doi.org/10.1002/ana.21107.
6. Campen CJ, Gutmann DH. Optic pathway gliomas in neurofibromatosis type 1. J Child Neurol. 2018;33:73–81. https://doi.org/10.1177/0883073817739509.
7. Sturgess B, Brown M, Fraser F, Bailey S. "They've got a lot of needs and I don't think they're being met fully": a qualitative study of the multi-professional team approach to the management of children with optic pathway gliomas. Pediatr Blood Cancer. 2018;65:e27377. https://doi.org/10.1002/pbc.27377.
8. Karaconji T, Whist E, Jamieson RV, Flaherty MP, Grigg JRB. Neurofibromatosis type 1: review and update on emerging therapies. Asia Pac J Ophthalmol (Phila). 2019;8(1):62–72. https://doi.org/10.22608/APO.2018182.
9. Rasool N, Odel JG, Kazim M. Optic pathway glioma of childhood. Curr Opin Ophthalmol. 2017;28:289–95. https://doi.org/10.1097/ICU.0000000000000370.
10. Bilgic S, Erbengi A, Tinaztepe B, Onol B. Optic glioma of childhood: clinical, histopathological, and histochemical observations. Br J Ophthalmol. 1989;73:832–7. https://doi.org/10.1136/bjo.73.10.832.
11. Avery RA, Fisher MJ, Liu GT. Optic pathway gliomas. J Neuroophthalmol. 2011;31:269–78. https://doi.org/10.1097/WNO.0b013e31822aef82.
12. Jahraus CD, Tarbell NJ. Optic pathway gliomas. Pediatr Blood Cancer. 2006;46:586–96. https://doi.org/10.1002/pbc.20655.
13. Wisoff JH, Abbott R, Epstein F. Surgical management of exophytic chiasmatic-hypothalamic tumors of childhood. J Neurosurg. 1990;73:661–7. https://doi.org/10.3171/jns.1990.73.5.0661.
14. Goodden J, Pizer B, Pettorini B, Williams D, Blair J, Didi M, et al. The role of surgery in optic pathway/hypothalamic gliomas in children. J Neurosurg Pediatr. 2014;13:1–12. https://doi.org/10.3171/2013.8.PEDS12546.
15. Liu Y, Hao X, Liu W, Li C, Gong J, Ma Z, et al. Analysis of survival prognosis for children with symptomatic optic pathway gliomas who received surgery. World Neurosurg. 2018;109:e1–e15. https://doi.org/10.1016/j.wneu.2017.09.144.
16. Ananias HJ, Yu Z, Dierckx RA, van der Wiele C, Helfrich W, Wang F, et al. (99m)Technetium-HYNIC(tricine/TPPTS)-Aca-bombesin(7-14) as a targeted imaging agent with microSPECT in a PC-3 prostate cancer xenograft model. Mol Pharm. 2011;8:1165–73. https://doi.org/10.1021/mp200014h.
17. Reubi JC, Korner M, Waser B, Mazzucchelli L, Guillou L. High expression of peptide receptors as a novel target in gastrointestinal

stromal tumours. Eur J Nucl Med Mol Imaging. 2004;31:803–10. https://doi.org/10.1007/s00259-004-1476-2.
18. Heuser M, Schlott T, Schally AV, Kahler E, Schliephake R, Laabs SO, et al. Expression of gastrin releasing peptide receptor in renal cell carcinomas: a potential function for the regulation of neoangiogenesis and microvascular perfusion. J Urol. 2005;173:2154–9. https://doi.org/10.1097/01.ju.0000158135.26893.bc.
19. Van de Wiele C, Dumont F, Dierckx RA, Peers SH, Thornback JR, Slegers G, et al. Biodistribution and dosimetry of (99m)Tc-RP527, a gastrin-releasing peptide (GRP) agonist for the visualization of GRP receptor-expressing malignancies. J Nucl Med. 2001;42:1722–7.
20. Van de Wiele C, Phonteyne P, Paillasse P, Goethals I, Van den Broecke R, Cocquyt V, et al. Gastrin-releasing peptide receptor imaging in human breast carcinoma versus immunohistochemistry. J Nucl Med. 2008;49:260–4. https://doi.org/10.2967/jnumed.107.047167.
21. Stoykow C, Erbes T, Maecke HR, Bulla S, Bartholoma M, Mayer S, et al. Gastrin-releasing peptide receptor imaging in breast cancer using the receptor antagonist (68)Ga-RM2 and PET. Theranostics. 2016;6:1641–50. https://doi.org/10.7150/thno.14958.
22. Maina T, Bergsma H, Kulkarni HR, Mueller D, Charalambidis D, Krenning EP, et al. Preclinical and first clinical experience with the gastrin-releasing peptide receptor-antagonist [68Ga]SB3 and PET/CT. Eur J Nucl Med Mol Imaging. 2016;43:964–73. https://doi.org/10.1007/s00259-015-3232-1.
23. Nock BA, Kaloudi A, Lymperis E, Giarika A, Kulkarni HR, Klette I, et al. Theranostic perspectives in prostate cancer with the gastrin-releasing peptide receptor antagonist NeoBOMB1: preclinical and first clinical results. J Nucl Med. 2017;58:75–80. https://doi.org/10.2967/jnumed.116.178889.
24. Nicolas GP, Morgenstern A, Schottelius M, Fani M. New developments in peptide receptor radionuclide therapy. J Nucl Med. 2019;60:167–71. https://doi.org/10.2967/jnumed.118.213496.
25. Zhang J, Niu G, Fan X, Lang L, Hou G, Chen L, et al. PET using a GRPR antagonist (68)Ga-RM26 in healthy volunteers and prostate cancer patients. J Nucl Med. 2018;59:922–8. https://doi.org/10.2967/jnumed.117.198929.
26. Flores DG, Meurer L, Uberti AF, Macedo BR, Lenz G, Brunetto AL, et al. Gastrin-releasing peptide receptor content in human glioma and normal brain. Brain Res Bull. 2010;82:95–8. https://doi.org/10.1016/j.brainresbull.2010.02.014.
27. Zhang J, Li D, Lang L, Zhu Z, Wang L, Wu P, et al. 68Ga-NOTA-aca-BBN(7-14) PET/CT in healthy volunteers and glioma patients. J Nucl Med. 2016;57:9–14. https://doi.org/10.2967/jnumed.115.165316.
28. Li D, Zhang J, Chi C, Xiao X, Wang J, Lang L, et al. First-in-human study of PET and optical dual-modality image-guided surgery in glioblastoma using (68)Ga-IRDye800CW-BBN. Theranostics. 2018;8:2508–20. https://doi.org/10.7150/thno.25599.
29. Dodge HW Jr, Love JG, Craig WM, Dockerty MB, Kearns TP, Holman CB, et al. Gliomas of the optic nerves. AMA Arch Neurol Psychiatry. 1958;79:607–21.
30. Wang H, Hou B, Lu L, Feng M, Zang J, Yao S, et al. PET/MRI in the diagnosis of hormone-producing pituitary microadenoma: a prospective pilot study. J Nucl Med. 2018;59:523–8. https://doi.org/10.2967/jnumed.117.191916.
31. Louis DN, Perry A, Reifenberger G, von Deimling A, Figarella-Branger D, Cavenee WK, et al. The 2016 World Health Organization Classification of Tumors of the Central Nervous System: a summary. Acta Neuropathol. 2016;131:803–20. https://doi.org/10.1007/s00401-016-1545-1.
32. Miyamoto J, Sasajima H, Owada K, Mineura K. Surgical decision for adult optic glioma based on [18F]fluorodeoxyglucose positron emission tomography study. Neurol Med Chir (Tokyo). 2006;46:500–3. https://doi.org/10.2176/nmc.46.500.
33. Moharir M, London K, Howman-Giles R, North K. Utility of positron emission tomography for tumour surveillance in children with neurofibromatosis type 1. Eur J Nucl Med Mol Imaging. 2010;37:1309–17. https://doi.org/10.1007/s00259-010-1386-4.
34. Goodden J. Optic pathway hypothalamic glioma. In: Winn HR, editor. Youmans and Winn neurological surgery. 7th ed. Philadelphia: Elsevier; 2016.
35. Beres SJ, Avery RA. Optic pathway gliomas secondary to neurofibromatosis type 1. Semin Pediatr Neurol. 2017;24:92–9. https://doi.org/10.1016/j.spen.2017.04.006.
36. Binning MJ, Liu JK, Kestle JR, Brockmeyer DL, Walker ML. Optic pathway gliomas: a review. Neurosurg Focus. 2007;23:E2. https://doi.org/10.3171/FOC-07/11/E2.
37. Guillamo JS, Creange A, Kalifa C, Grill J, Rodriguez D, Doz F, et al. Prognostic factors of CNS tumours in neurofibromatosis 1 (NF1): a retrospective study of 104 patients. Brain. 2003;126:152–60. https://doi.org/10.1093/brain/awg016.
38. Jittapiromsak N, Hou P, Liu HL, Sun J, Slopis JM, Chi TL. Prognostic role of conventional and dynamic contrast-enhanced MRI in optic pathway gliomas. J Neuroimaging. 2017;27:594–601. https://doi.org/10.1111/jon.12450.
39. Maloney E, Stanescu AL, Perez FA, Iyer RS, Otto RK, Leary S, et al. Surveillance magnetic resonance imaging for isolated optic pathway gliomas: is gadolinium necessary? Pediatr Radiol. 2018;48:1472–84. https://doi.org/10.1007/s00247-018-4154-4.